Martin–Luther–Universität
Halle–Wittenberg
Institut für Mathematik

Bifurcations and synchronization of singularly perturbed oscillators: an application case study

H. Podhaisky and W. Marszalek

Report No. 01 (2011)

Editors:
Professors of the Institute for Mathematics, Martin-Luther-University Halle-Wittenberg.

Electronic version: see `http://www2.mathematik.uni-halle.de/institut/reports/`

Bifurcations and synchronization of singularly perturbed oscillators: an application case study

H. Podhaisky and W. Marszalek

Report No. 01 (2011)

Helmut Podhaisky
Martin-Luther-Universität Halle-Wittenberg
Naturwissenschaftliche Fakultät II
Institut für Mathematik
Theodor-Lieser-Str. 5
D-06120 Halle/Saale, Germany
Email: helmut.podhaisky@mathematik.uni-halle.de

W. Marszalek
DeVry University
College of Engineering and Information Sciences
630 US Highway 1, North Brunswick, NJ 08902, USA
Email: wmarszalek@devry.edu

Technical Report

Bifurcations and synchronization of singularly perturbed oscillators: an application case study

Helmut Podhaisky · Wieslaw Marszalek

May 18, 2011

Abstract We present numerically obtained bifurcations of two dual singularly perturbed nonlinear oscillating circuits. Each of the circuits comprises two coupled sections: a nonlinear section with dissipation and a linear one with a small constant biasing source. The two dual oscillators show an interesting pattern of hierarchical oscillations that follow the Stern-Brocot tree with intervals of synchronization yielding Arnold's tongues and their corresponding devil's-like staircases. Several numerical results are included.

Keywords Bifurcations · Mixed-mode oscillations · Entrainment modes · Arnold's tongues · Devil's staircases · Chaos · Event location in ODEs

1 Introduction

Consider two dual circuits shown in Fig.1. Each circuit includes one nonlinear element with a cubic current-voltage characteristics, either $V_{nonl} = \alpha x_1^2 + \beta x_1^3$, or equivalently $I_{nonl} = \alpha x_1^2 + \beta x_1^3$, where $\alpha > 0$, $\beta < 0$. Also, each circuit has one linear controlled element, V or I, respectively, and a constant biasing source a. All other elements in both circuits are linear. Varying the values of conductance G (or resistance R) in the circuits in Fig.1 changes the coupling between the left and right sections of each circuit with the strongest coupling at $G = 0$ ($R = 0$). The coupling becomes weaker with increased G (or R). The right section of each circuit is a linear oscillator serving as a driver of the left section which is a nonlinear oscillator.

If we assume (see Fig.1) that $0 < L_1 \equiv \epsilon \ll 1$ and $C, L_3 \sim \mathcal{O}(1)$ ($0 < C_1 \equiv \epsilon \ll 1$ and $L, C_3 \sim \mathcal{O}(1)$), then the circuits can be described by the following set

H. Podhaisky is with Martin-Luther-Universität Halle-Wittenberg, Institut für Mathematik, Theodor-Lieser-Str. 5, 06120 Halle (Saale), Germany. Tel.: +49-345-55-24660, E-mail: helmut.podhaisky@mathematik.uni-halle.de. **W. Marszalek** (corresponding author) is with DeVry University, College of Engineering and Information Sciences, 630 US Highway 1, North Brunswick, NJ 08902, USA. Tel.: +001-732-729-3935, E-mail: wmarszalek@devry.edu.

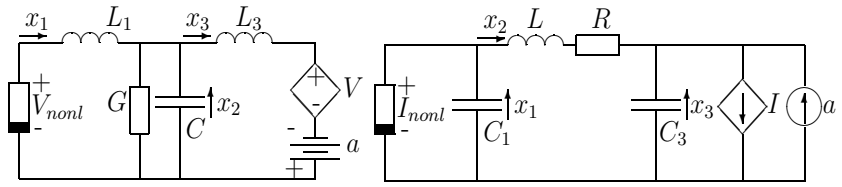

Fig. 1 Left: The LCL circuit with $L_1 = \epsilon \ll 1$, $V = (1+b)x_2$, $V_{nonl} = \alpha x_1^2 + \beta x_1^3$. Right: The CLC circuit with $C_1 = \epsilon \ll 1$, $I = (1+b)x_2$, $I_{nonl} = \alpha x_1^2 + \beta x_1^3$. For both circuits: $a > 0$, $b > 0$, $\beta < 0$ and $\alpha > 0$.

of singularly perturbed ODEs

$$\begin{aligned} \epsilon x_1' &= -x_2 + \alpha x_1^2 + \beta x_1^3 \equiv g(x_1, x_2, x_3) \\ x_2' &= x_1 - x_3 - K x_2 \quad \equiv f_1(x_1, x_2, x_3) \\ x_3' &= a - b x_2 \qquad\quad \equiv f_2(x_1, x_2, x_3) \end{aligned} \tag{1}$$

where $K \equiv G$ for the circuit on the left side in Fig.1 and $K \equiv R$ for the circuit on the right side in Fig.1.

Each parameter of the circuits, a, b, α, β, G (R) and ϵ, has a significant impact on various dynamical properties of the circuits.

The singularly perturbed model (1) with $K = 0$ was analyzed from the point of view of its mixed-mode oscillations (or MMOs) in [1]. The circuits were originally introduced in [2] and their L^s-type bifurcation diagrams were presented in [3] with the pair of coprime integers (L, s) denoting the numbers of large and small amplitude oscillations, respectively. The MMOs of type L^s occur when a synchronization (also called the entrainment or injection locking) phenomenon of two oscillators occurs. Several bifurcation diagrams with slowly varying parameters a, b, α and β show intriguing patterns of the L^s sequences when the linear and nonlinear sections of the circuits are locked.

The MMOs and synchronization phenomena are widely present in many biological and chemical systems (see e.g. [4]). Human heart may experience cardiac dysrhythmias resulting from a lack of synchronization of various pacemaker sites in the heart. Such problems can often be identified with a routine electrocardiogram (ECG) scan [5]. Other important areas of injection locking and synchronization phenomenon are the epileptic brain cell diseases (e.g. seizures) resulting from a synchronization of a massive population of neurons in human brain. Such synchronization (that is in some sense equivalent to the L^s-type of MMOs studied in this paper) can be monitored by EEG [6].

In this paper we present numerically obtained results on synchronization phenomenon in the two circuits presented above. In particular, we examine various parameters of the circuits and their impact on the shape of Arnold's tongues, peak-to-peak maps and devil's staircases. We believe that the results presented in this paper shed a new light on the general properties of the mathematical model (1) and the circuits in Fig.1 in particular. The present paper complements those earlier results and shows further interesting properties of the two circuits by using a variety of numerical results obtained by using our in-home bifurcation software (based on Fortran and Python), see appendix A for a short description of `bif.f90`.

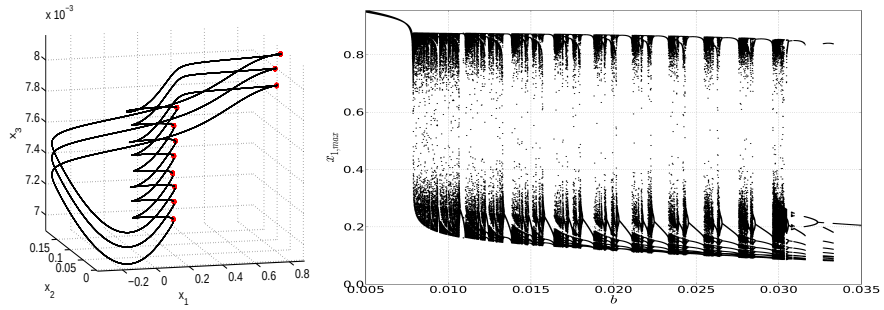

(a) (b)

Fig. 2 (a) Typical periodic L^s ($L = 3$, $s = 8$). (b) Bifurcation diagram $x_{1,max}$ versus b with $a = 0.0005$, $\alpha = 1$, $\beta = -1$. For both graphs $K = 0.3$ and $\epsilon = 0.01$.

The interested readers are welcome to request (from the first author) a copy of the software that was used to create all graphs in this paper.

2 Details of the numerical approach

The system (1) exhibits a very rich dynamical behavior. To be able to study it in detail, one needs a computational tool which can accurately and efficiently determine the L^s-type of MMOs the system may show for certain parameter values. For this we have written a Fortran-90 code `bif.f90` as follows.

The system (1) is integrated with the fifth order Runge-Kutta (RK) method of [8]. The step size selection is based on local error estimation with tolerances $ATOL = RTOL = 10^{-8}$. Starting from $x_1(0) = x_2(0) = x_3(0) = 0$, we integrate the system until $t_{end} = 500$, but the local maxima of $x_1(t)$ are detected in the interval from $t_{trans} = 300$ until t_{end}. The crucial part of the algorithm is the computation of the event points t^* with $x_1'(t^*) = 0$. For this we exploit the fourth order continuous extension of the RK method [9] given as the polynomial $x_1(t_m + \theta h) = p_m(\theta) \equiv x_1(t_m) + h\sum_{i=1}^{s} b_i(\theta)\frac{1}{\epsilon}g_i$, where $b_i(\theta)$ is the weight (polynomial) of the RK formula for $t = t_m + h\theta$, g_i denotes the value of g in (1) evaluated at stage i and $s = 7$ is the number of stages. We find $t^* = t_m + h\theta$ by computing the roots $\theta \in [0, 1]$ of the polynomial $p_m'(\theta)$ using LAPACK's general eigenvalue solver `dgeev` and then checking if $p_m''(\theta) < 0$ holds true. The use of eigenvalue solvers for event location in initial-value problems is discussed in details in [7]. Let T^* denotes the set of all t^* found by this procedure. Finally, to determine L^s, we cluster the points $X^* = \{x(t) : t \in T^*\}$ using their Euclidean distance as the separation criterion. For this we consider the $x(t_1^*)$ and $x(t_2^*)$ as lying on the same trajectory, if $\|x(t_1^*) - x(t_2^*)\|_2 < d$. In all our computation we used the threshold $d = 10^{-4}$.

To comment on computing times, let's consider the calculation of a single solution of (1) for $t \in [0, 500]$. We choose parameters $a = 0.0005$, $b = 0.017$, $K = 0.3$, $\alpha = 1$, $\beta = -1$ and $\epsilon = 0.01$ corresponding to a 3^7-type MMO. The time integration needs $50,653$ steps for which the running time is about 0.6 seconds on an PC (Intel Pentium processor with 2.4 GHz running under Linux). Doing the same calculation to the same accuracy in MATLAB it takes about 23 seconds

on the same computer. Since we had to repeat such computations with different parameter values millions of times, we also used an IBM575 computing server. A single core of this machine (Power-6, clocked 4.7 GHz) needs about 0.3 seconds for one run. We used up to 30 cores simultaneously, leading to an effective speed-up of more than 2000 times compared with MATLAB. The figures have been created directly from the output of `bif.f90` using Python with the Matplotlib toolbox. We used 10^4 parameter values to plot each of the bifurcation diagrams (Figs.2(b) and 9) and $10^3 \times 10^3$ grid points to plot Arnold's tongues (Figs.3,5,6,8,10(a),(b),12).

3 Synchronization of oscillators: Arnold's tongues

The linear part of each of the dual circuits (with a small biasing voltage (or current) source with value a) serves as a driving circuit. For the given values of α, β and K, the two other parameters, namely a and b, play a pivotal role in determining the frequency and amplitude of the periodic signal generated in the linear part. It has been shown that for $K = 0$ (full strength coupling) and fixed α and β the circuits will be in the MMOs mode (either periodic, quasi-periodic or chaotic) if [2]

$$4b\alpha^3/(27\beta^2) - 1/(8\alpha) < a < b\alpha^3/(18\beta^2). \tag{2}$$

The period of small amplitude oscillations in the sequence L^s has also been estimated in [2] as $T = 2\pi/\sqrt{\epsilon^{-1} - b}$, and since, typically, $b \sim \mathcal{O}(\epsilon)$, therefore $T \approx 2\pi\sqrt{\epsilon}$. Fig.2(a) shows typical L^s periodic MMOs. Fig.2(b) on the other hand, shows that periodic MMOs L^s (for various pairs of integers L and s) occur only if the slowly varying parameter b is within certain intervals. These intervals are separated by other intervals of different nature where either the quasi-periodic, period doubling (or halving), or chaotic responses occur. The lengths and center points of the intervals of parameter b with purely periodic responses L^s change with parameter K. The parameter K represents the strength of coupling between the linear and nonlinear sections of each circuit, therefore the location and length of the intervals of b with purely periodic L^s oscillations is a function of K. Plotting such intervals of b against K yields the famous Arnold's tongues [10], [11]. Fig.3 shows several Arnold's tongues for the dual circuits obtained for $0 \le K \le 4$ while the rest of parameters is the same as in Fig.2(b). In graphing all the tongues 1^k in Fig.3 we combined together both the coprime and noncoprime pairs of L and s. For example, the light blue color (online) was used to graph the tongues 1^5, 2^{10}, 3^{15} and 4^{20}, while the dark blue color (online) was used for the tongues 1^7, 2^{14}, 3^{21} and 4^{28}. The maximum L value used in plotting Fig.3 was 4. Note that the pairs of L and s values within each L^s group (we call it the *major* tongue) reduce to the same L/s ratio (also called the winding number). Fig.4 shows two major tongues 1^6 and 1^7 extracted from Fig.3 with separated coprime and noncoprime tongues within each major tongue. The maximum L value used in plotting Fig.4 was 6. Fig.3 can further be filled up with other major tongues with $L > 1$. This is illustrated in Fig.5 which shows all the major tongues 1^k $(k = 1, \ldots, 9)$, 2^l $(l = 1, 3, 5, \ldots, 17)$ and 3^m $(m = 1, 2, 4, 5, \ldots, 26)$. Within any of the major tongues 2^l and 3^m there exist some tongues with noncoprime pairs of L and s, in the same way as it was described above for the major tongues 1^5 and 1^7. Fig.6 shows the detailed tongues L^s with both coprime and noncoprime integers L and s

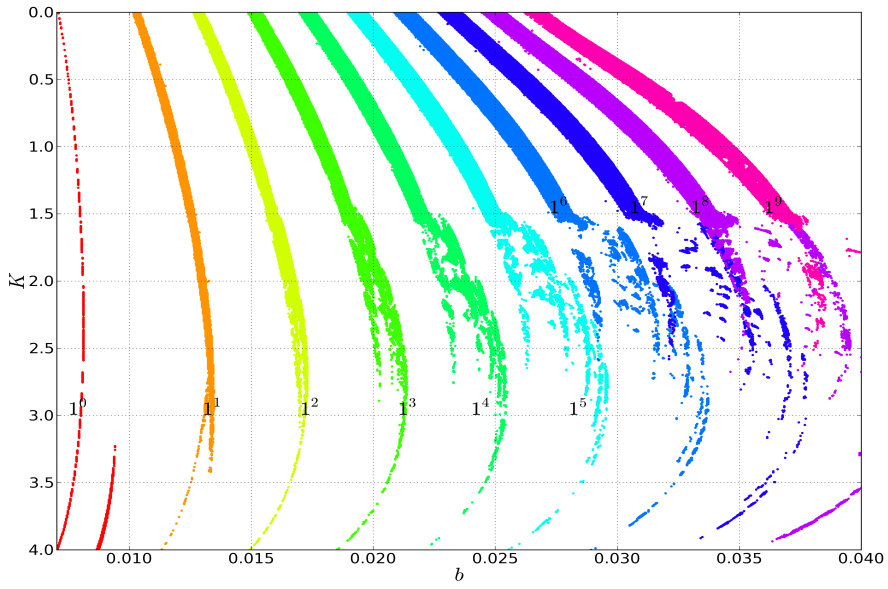

Fig. 3 Numerically obtained Arnold's tongues 1^k, $k = 1, \ldots, 9$.

within the rectangular box marked in Fig.5. Further addition of the tongues with larger L and s values is also possible.

An interesting picture can be drawn from the analysis of the major tongues occurring when b changes slowly (up to approximately the value of 0.03). Namely, the major tongues L^s with coprime L and s can schematically be represented for the first 4 layers (that is with $L = 1, \ldots, 4$) as follows

$$\begin{array}{ll} L=1: & 1^0, 1^1, 1^2, 1^3, 1^4, 1^5, 1^6, 1^7, 1^8, 1^9 \\ L=2: & 2^1, 2^3, 2^5, 2^7, 2^9, 2^{11}, 2^{13}, 2^{15}, 2^{17} \\ L=3: & 3^1, 3^2, 3^4, 3^5, 3^7, 3^8, 3^{10}, 3^{11}, 3^{13}, 3^{14}, 3^{16}, 3^{17}, 3^{19}, 3^{20}, 3^{22}, 3^{23}, 3^{25}, 3^{26} \\ L=4: & 4^1, 4^3, 4^5, 4^7, 4^9, 4^{11}, 4^{13}, 4^{15}, 4^{17}, 4^{19}, 4^{21}, 4^{23}, 4^{25}, 4^{27}, 4^{29}, 4^{31}, 4^{33}, 4^{35} \\ \ldots & \ldots \end{array} \tag{3}$$

If we use $L/(L+s)$ (called the firing number) rather L/s, then all the major tongues above can be graphically represented by the well-known Stern-Brocot tree of coprime integers L and s yielding the firing number between 0 and 1 [12]. Such pairs of coprime integers follow Farey arithmetic: if $L_1^{s_1}$ and $L_2^{s_2}$ are two *parent* tongues, then their *daughter* tongue is $(L_1 + L_2)^{s_1+s_2}$. For example, the *daughter* tongue 2^3 has 1^1 and 1^2 as her *parent* tongues, while the 1^1 and 2^3 are the *parent* tongues for the 3^4 *daughter* tongue. Furthermore, the 1^1 and 3^4 tongues are the *parents* of 4^5, etc. (see Fig.6). Interesting graphs of different versions of the Stern-Brocot tree with descriptions of their origins and properties (e.g. relation to the Fibonacci sequence) can be found in [13].

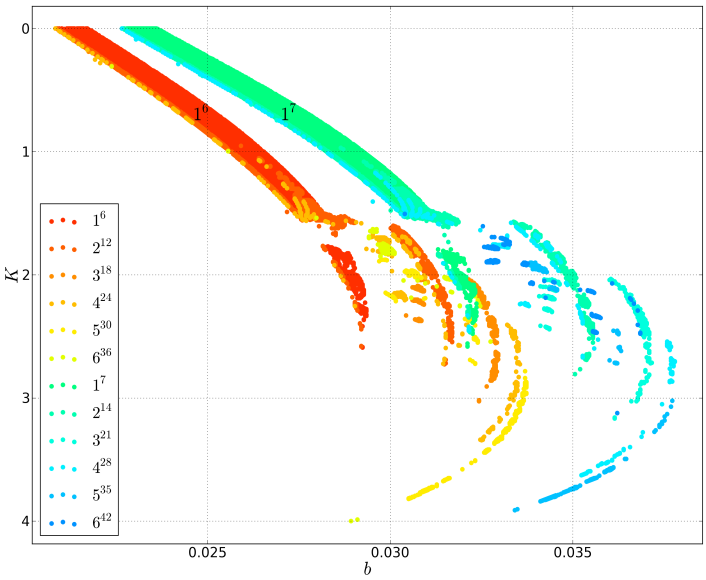

Fig. 4 Arnold's tongues 1^6 and 1^7 with their coprime and noncoprime components.

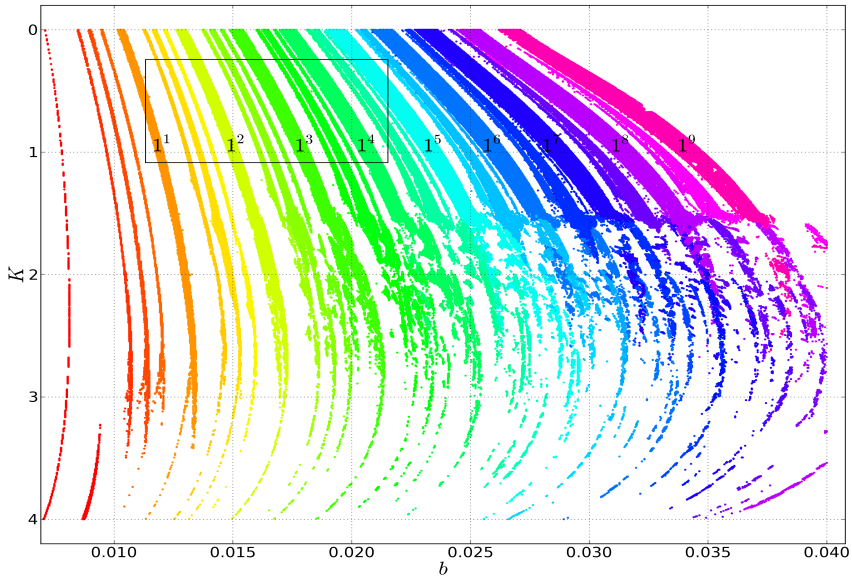

Fig. 5 Major tongues 1^k $(k = 1, \ldots, 9)$, 2^l $(l = 1, 3, 5, \ldots, 17)$ and 3^m $(m = 1, 2, 4, 5, \ldots, 26)$.

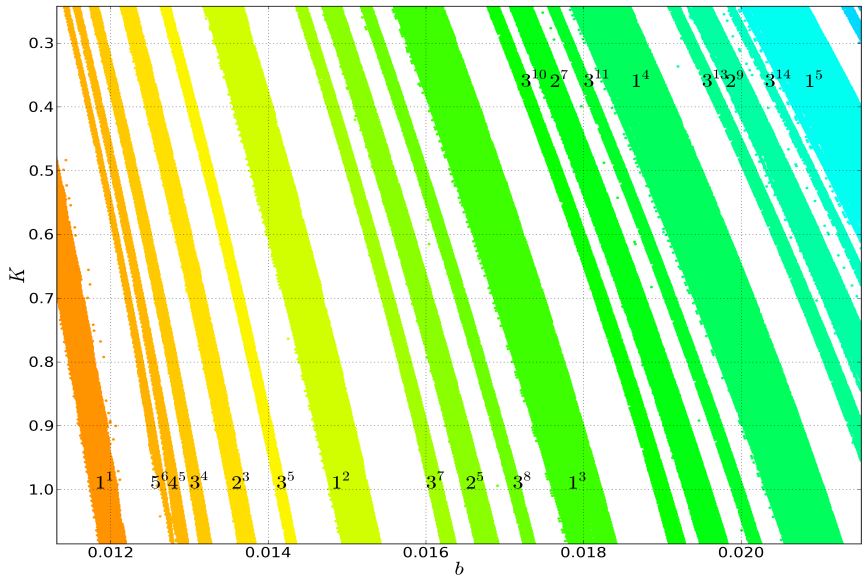

Fig. 6 Detailed tongues L^s within the rectangular box in Fig.5. The white strips contain other *higher-order* tongues with relatively narrow widths.

If $b > 0.03$ in Fig.2(b), then the sequence of chaotic and period oscillations is rather peculiar and does not follow the pattern of sequences for $b < 0.03$. To the right of the interval of periodic oscillations 1^9 one can find the following sequence of periodic oscillations 1^{10}, 0^2, 0^1, 1^{11} and 0^1 with the corresponding sequence of the firing numbers (including the 1^9 sequence): $1/10, 1/11, 0, 0, 1/12, 0$. This sequence is not nonincreasing as it would normally be, should the L^s sequence follow Farey arithmetic, as, for example, shown in Fig.6. Fig.7 shows the devil's-like staircase of the $L/(L+s)$ values versus b obtained from Fig.5 at the $K = 0.3$ level. The nonmonotonic nature of such a staircase is clearly seen from both graphs shown in Fig.7. This phenomenon, rather unexpected, indicates that while, in general, the circuits obey the rules of Farey arithmetic, there are also intervals of b (of rather short width) where such rules are not obeyed by (1).

4 Bifurcation with other parameters and the role of dissipation

4.1 Parameters a, α and β

Bifurcation diagrams and Arnold's tongues similar to those presented in the previous section with varying parameter b also exist when parameters a, α or β are varied. The parameter a controls the periodic signal coming out of the linear section in the circuits (just like the parameter b does), therefore the nature of the bifurcation process for parameter a is very similar to that of parameter b with

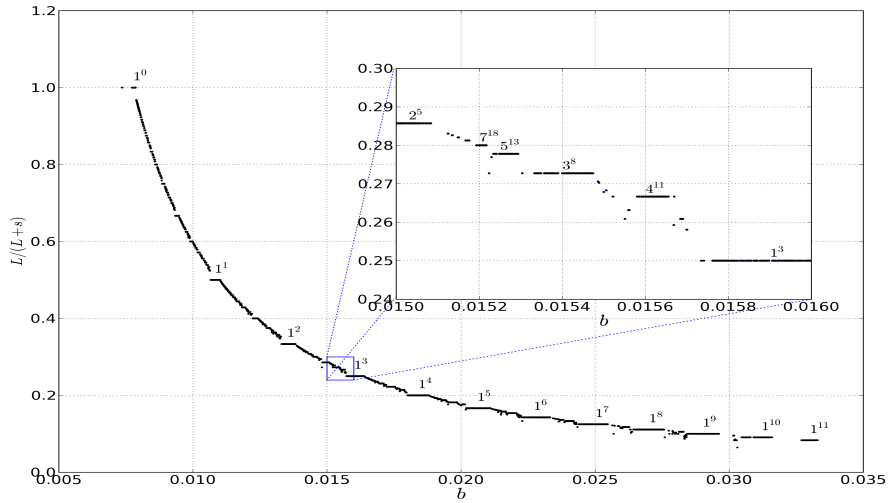

Fig. 7 The $L/(L+s)$ staircase for $a = 0.0005$, $\alpha = 1$, $\beta = -1$, $\epsilon = 0.01$ and $K = 0.3$.

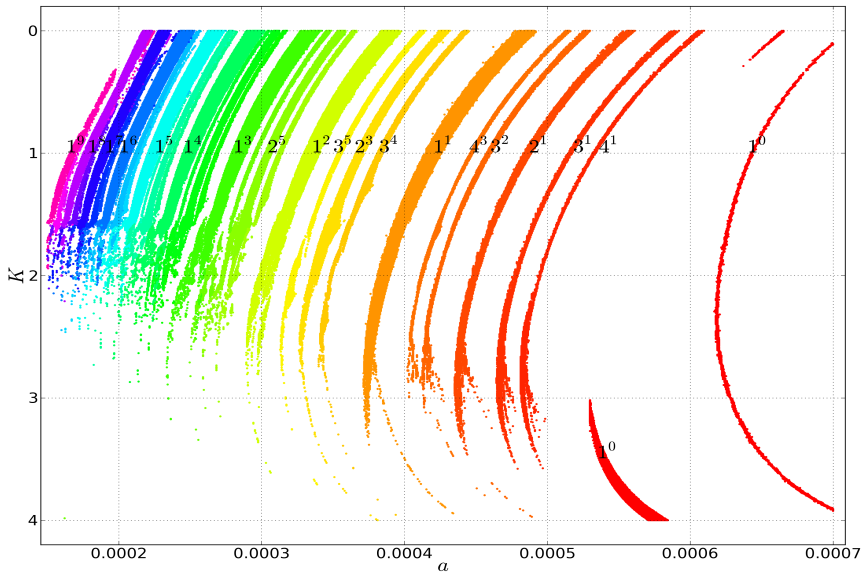

Fig. 8 Major Arnold's tongues with varying parameter a.

the 1^0 and 0^1 MMOs interchanged. Fig.8 shows three layers of the major Arnold's tongues L^s with $L = 1, 2, 3$ when a varies slowly.

When parameters α or β are varied we obtain slightly different bifurcation diagrams and their Arnold's tongues. These two parameters shape out the nonlinear section of each circuit. Two bifurcation diagrams for α and β and their corresponding Arnold's tongues are shown in Figs.9 and 10, respectively. They extend to the right, while the most important portion of the figures (with the largest intervals of synchronization of type L^1) is between the 1^0 and 1^1 MMOs. The synchronization intervals to the right of 1^1 are much narrower than those on the left side of 1^1.

Finally, an example of Arnold's tongues with both parameters a and b varying is shown in Fig.11. This figure is consistent with the 1^s diagram, that is Fig.11 in [2], and with the conjecture on the lengths of the sectors of rotation for secondary canards, i.e. solutions with small oscillations in [1].

4.2 Dissipation

Dynamical behavior of the dual circuits considered in this paper shows a striking similarity with other systems considered in the literature, in particular in various oscillators synchronized by an external periodic force. Such examples include the well-known Duffing oscillator with dissipation, the forced damped pendulum, the Wien bridge connected to an electrochemical cell and others [14–16]. In a relatively simple general case, such oscillators with external sinusoidal forcing can be described by the following equation

$$x'' + R_d(x)x' + dV(x)/dx = p(t) \tag{4}$$

where $R_d(x)$ is the dissipation and $p(t)$ is an external periodic sinusoidal force with certain amplitude and frequency. The $V(x)$ denotes the potential function of the system. External non-sinusoidal periodic forces are also possible (see e.g. [17]).

Our circuits are more complicated than the systems described by (4). It can be shown that the variable $x_1(t)$ in (1) satisfies equation analogous to (4) with $p(t) = \epsilon^{-1}x_3(t)$, as follows

$$x_1'' + (K - \epsilon^{-1}(2\alpha x_1 + 3\beta x_1^2))x_1' + \epsilon^{-1}(x_1 - K(\alpha x_1^2 + \beta x_1^3)) = \epsilon^{-1}x_3(t) \tag{5}$$

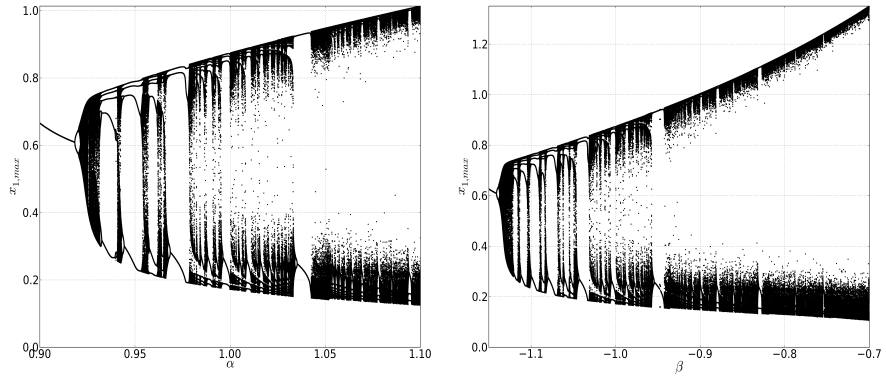

(a) (b)

Fig. 9 Bifurcation diagrams for $K = 0.3$ and varying parameter α (a) and β (b).

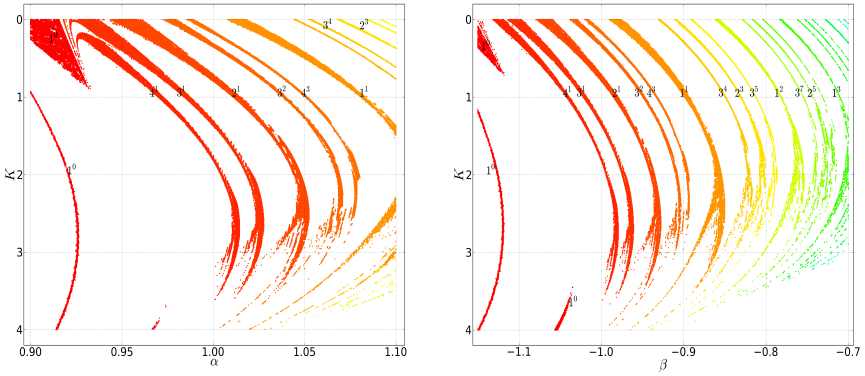

(a) (b)

Fig. 10 Arnold's tongues for $K = 0.3$ and parameter α (a) and β (b).

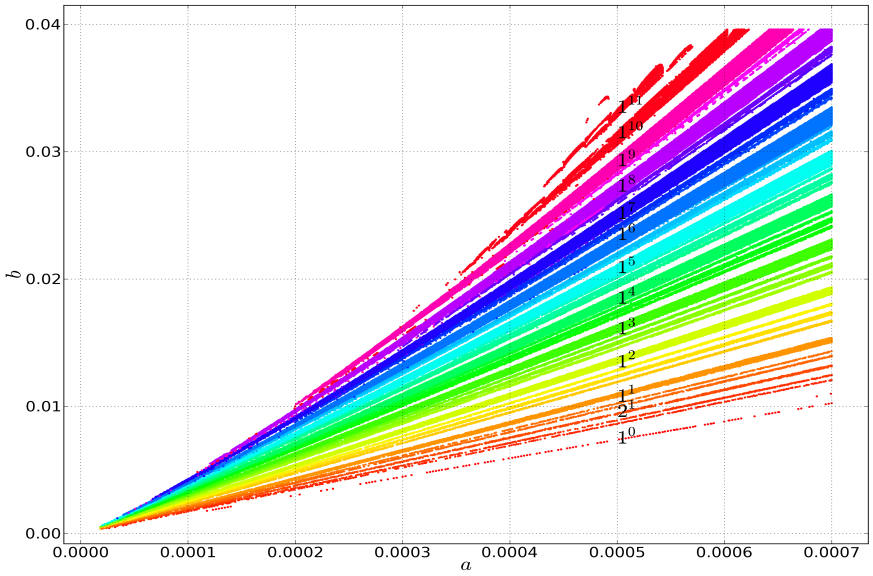

Fig. 11 Arnold's tongues with varying parameters a and b for $K = 0.3$.

which is coupled with the following first-order equation

$$x_3' - b\epsilon x_1' = a - b(\alpha x_1^2 + \beta x_1^3) \tag{6}$$

from which we obtain[1] $R_d(x_1) = K - \epsilon^{-1}(2\alpha x_1 + 3\beta x_1^2)$ and $dV(x)/dx = \epsilon^{-1}(x_1 - K(\alpha x_1^2 + \beta x_1^3))$. For fixed ϵ, α and β the coefficient $R_d(x_1)$ varies with x_1 and K.

[1] Alternatively, one can consider the second-order equation $x_3'' + Kx_3' - bx_3 = Ka - x_1$ coupled with (6).

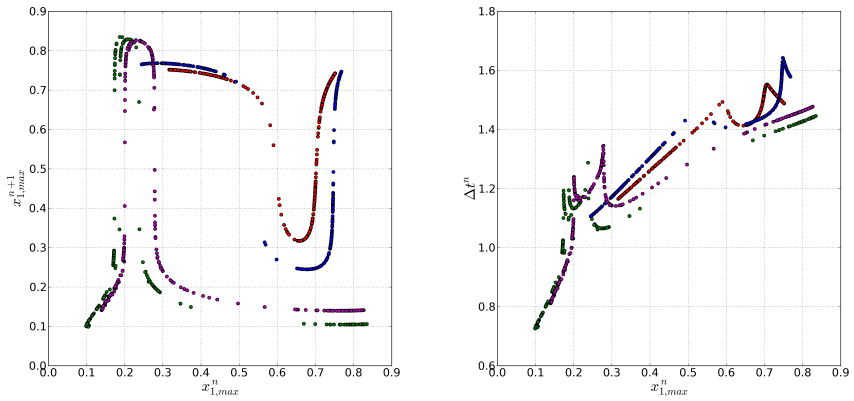

(a) (b)

Fig. 12 (a) Peak-to-peak and (b) return-time plots. Color red (online): $a = 0.0005$, $b = 0.01$, $\alpha = 0.93$, $K = 0.3$; blue: $a = 0.0005$, $b = 0.01$, $\alpha = 0.942$, $K = 0$; green: $a = 0.0005$, $b = 0.0256$, $\alpha = 1$, $K = 0.3$; magenta: $a = 0.00024$, $b = 0.01$, $\alpha = 1$, $K = 0$. For all plots $\beta = -1$ and $\epsilon = 0.01$

Typically, $R_d(x_1)$ changes sign in time. In general, increasing K increases damping $R_d(x_1)$ and therefore reduces synchronization of the linear and nonlinear sections of the oscillators. The tongues become narrower as it can be clearly seen from Figs.3-6. Another way of increasing damping is to add an additional resistor, say R_{dis}, in series with the inductor L_1 in the circuit on the left side in Fig.1, or, equivalently, an additional conductance G_{dis} parallel to the capacitor C_1 in the circuit on the right side in Fig.1. Assuming that $K_{dis} = G_{dis}$ (or $K_{dis} = R_{dis}$), such an addition is, in fact, equivalent to having the V_{nonl} (or equivalently I_{nonl}) in the form $K_{dis}x_1 + \alpha x_1^2 + \beta x_1^3$. For fixed α and β increasing K_{dis} reduces the amplitudes of small oscillations and also the widths of Arnold's tongues.

4.3 Peak-to-peak and return-time plots

Two very important plots can be drawn for our circuits operating in chaotic cases: the peak-to-peak and return-time plots. These two plots can be used to find a reduced order model (or peak-to-peak map) for a chaotic system, which, in turn, allows solving important problems of optimal control of the chaotic system under consideration. For a chaotic attractor with variable x(t) and the peak values x^n occurring at time instants t_n $(n = 1, 2, \ldots)$ we draw the points (x^n, x^{n+1}) for the peak-to-peak plot and the points $(x^n, \Delta t^n)$, $\Delta t^n \equiv t_{n+1} - t_n$, for the return-time plot. Such plots comprise a finite number of distinct points for a purely periodic $x(t)$, while for a chaotic $x(t)$ the distinct points may align along a curve. Also, a quasiperiodic dynamics results in a closed curve. The peak-to-peak and return-time plots have been successfully obtained for the Lorentz, Chua, Rössler, Duffing, Newton-Leipnik and other oscillators [18]. Fig.12 shows four examples of each of the two plots for (1). Selecting different set of parameters for the circuits working in a chaotic regime results in different plots. Table 1 shows the Lyapunov

Table 1 The Lyapunov exponents and Kaplan-Yorke fractal dimensions D_{KY} and D_Σ for the chaotic attractors in Fig.12. The attractors are labeled by their colors (online) used in Fig.12.

Attractor	$\lambda_1, \lambda_2, \lambda_3$	D_{KY}	D_Σ
Red	3.7904, −0.0019, −8.1658	2.4639	2.5855
Blue	3.7554, −0.0019, −8.2038	2.4575	2.5796
Green	1.8093, −0.0001, −6.0506	2.2990	2.4209
Magenta	3.7271, −0.0001, −7.3562	2.5066	2.6240

exponents λ_i $(i = 1, 2, 3)$ corresponding to the four chaotic attractors' plots in Fig.12. The attractors' Kaplan-Yorke fractal dimensions D_{KY} and D_Σ [19] are also included. For a three variable nonlinear dynamical system with a strange attractor the Kaplan-Yorke dimension is found by numerically calculating the Lyapunov exponents λ_i, $i = 1, 2, 3$, and substituting them in the formula $D_{KY} = k + \frac{\Sigma_{i=1}^{k} \lambda_i}{|\lambda_{k+1}|}$ with k obtained from the following conditions: $\Sigma_{i=1}^{k} \lambda_i > 0$ and $\Sigma_{i=1}^{k+1} \lambda_i < 0$. The Lyapunov exponents are also used to calculate the modified Kaplan-Yorke fractal dimension, D_Σ, which, for a three variable chaotic flow with a strange attractor, equals $D_\Sigma = 1.5 + 0.5\sqrt{1 - 8\frac{\lambda_1}{\lambda_3}}$ with $D_\Sigma \geq D_{KY}$ for $-1 \leq \lambda_1/\lambda_3 \leq 1$. The maximum difference $D_\Sigma - D_{KY}$ is 1/8 and it occurs at $\lambda_1/\lambda_3 = -3/8$. The last column in Table 1 shows the values of D_Σ for the four chaotic strange attractors.

5 Conclusion

The computational results presented in this paper show striking similarities of the dynamical bifurcation properties of the two dual circuits with many oscillating systems in chemistry, biology, engineering and human organs (heart and brain). The periodic L^s MMOs result from the synchronization of the nonlinear and linear sections of the circuits. In practice, a synchronization is a desired outcome of using implanted human heart pacemakers. The synchronization of large population of neurons in human brain, may, on the other hand, cause epileptic seizures. The synchronized periods of various L^s MMOs with intermediate intervals of quasiperiodic and/or chaotic responses are typical features of epileptic seizures (see Figs.17.11 and 17.14 in [6]). Also typical features in such studies are Arnold's tongues and devil's staircases (Figs.7.11,8.1-8.3 in [6]). Further areas where the synchronization (entrainment) phenomena occur are the secure telecommunication transmission, electrochemical oscillators, human cardiorespiratory systems and others [20].

Acknowledgements The second author thanks the Alexander von Humboldt-Stiftung for a financial support during his research stay at Martin-Luther-Universität Halle-Wittenberg in Germany.

References

1. M. Krupa, N. Popovic, N. Kopell, Mixed-mode oscillations in three time-scale systems: a prototypical example, SIAM J. Appl. Dynam. Sys., 7, 361–420 (2008)
2. W. Marszalek, Z. Trzaska, Mixed-mode oscillations in a modified Chua's circuit, Circuits, Systems, Signal Proc., 29, 1075–1087 (2010)

3. W. Marszalek, Z. Trzaska, Mixed-mode oscillations and chaos in nonlinear circuits, Acta Technica, *to appear*, 56, no.2, (2011)
4. Focus issue, Mixed-Mode Oscillations: Experiment, Computation, and Analysis, Chaos, 18 (2008)
5. L. Glass, M. R. Guevera, A. Shrier, R. Perez, Bifurcation and chaos in a periodically stimulated cardiac oscillator, Physica, 7D, 89–101 (1983)
6. J. Milton, P. Jung (Eds.), Epilepsy as a Dynamic Disease, Springer-Verlag, Berlin Heidelberg (2003)
7. R. M. Corless, A. Shakoori, D. A. Aruliah, L. Gonzalez-Vega, Barycentric Hermite interpolants for event location in initial-value problems, J. Numer. Anal. Ind. Appl. Math., 3, 1–16 (2008)
8. J. R. Dormand, P.J. Prince, A family of embedded Runge-Kutta formulae, J. Comp. Appl. Math., 6, 19–26 (1980)
9. E. Hairer, S. P. Nørsett, G. Wanner, Solving Ordinary Differential Equations I, Springer-Verlag, Berlin Heidelberg (1993)
10. V. I. Arnold, Geometrical Methods in the Theory of Ordinary Differential Equations; M. Levy (Ed.), Grundlehren der Mathematischen Wissenschaften, 250, Springer-Verlag, New York (1983)
11. H. Mori, Y. Kuramoto, Dissipative Structures and Chaos, Springer-Verlag, New York (1997)
12. J. G. Freire, J. A. C. Gallas, Stern-Brocot trees in cascades of mixed-mode oscillations and canards in the extended Bonhoeffer-van der Pol and FitzHugh-Nagumo models of excitable systems, Physics Lett. A, 375, 1097–1103 (2011)
13. N. J. Wildberger, Evolution versus intelligent design: a mathematician's view, http:// web.maths.unsw.edu.au/∼norman/papers/Intelligent Designhtml /IntelligentDesign1.htm, (2008). Accessed 4 May 2011
14. A. L. Gama, M. S. T. de Freitas, Do Arnold tongues really constitute a fractal set? J. Physics, 246, 012031 (2010)
15. V. Paar, N. Pavin, Intermingled fractal Arnold tongues, Physical Review E, 57, 1544–1549 (1998)
16. S. Nakata, K. Miyazaki, S. Izuhara, H. Yamaoka, D. Tanaka, Arnold tongue of electrochemical nonlinear oscillators, J. Phys. Chem. A, 113, 6876–6879 (2009)
17. P. Bhansali, J. Roychowdhury, Gen-Adler: The generalized Adler's equation for injection locking analysis in oscillators, Proc. 14th ASP-DAC, Yokohama (Japan), 522–527 (2009)
18. C. Piccardi, S. Rinaldi, Optimal control of chaotic systems via peak-to-peak maps, Int. J. Bifurc. Chaos, 12, 2927–2936 (2002)
19. K. E. Chlouverakis, J. C. Sprott, A comparison of correlation and Lyapunov dimensions, Physica D. 200, 156–164 (2005)
20. M. McGuinness, Y. Hong, Arnold's tongues in human cardiorespiratory systems, Chaos, 14, 1–6 (2004)

A The code `bif.f90`

The code `bif.f90` has been written in Fortran-90 and it can be requested from the first author. Since `bif.f90` depends on the eivenvalue solver `dgeev` it has to be linked to LAPACK. To compile `bif.f90` under Linux use

```
gfortran -fopenmp -O4 -o bif bif.f90 -llapack
```

where the optional flag `-fopenmp` is used to enable parallelization.
The code `bif.f90` parses the command line arguments. If no arguments are given, it displays the following help message:

```
   ./bif [logfile=<filename>]  [<par>=left,right,npoints]
          [writelast100] [tend=tend] [transient=transient] [plot]

The parameters (with their default values) are:
   a (0.0005) , b (0.01), K (0.3) , alpha (1), beta (-1), epsilon (0.01).

Meaning of the flags:

  * writelast100:
      The last 100 values of x1max are also written
      to the output loc.txt (for drawing bifurcation diagrams)

  * plot : Viusualize. Applies only to fixed parameter (one-point) computations
```

The command line to compute and draw the solution of system (1) with parameter $b = 0.017$ is

```
./bif  b=0.017 plot
```

yielding the output

```
# ./bif b=0.017
# BIF -- $Revision: 1.16 $
#
 INTEGRATION
    50653 +   2910 steps,  196 nloc, 0.59 s
 CLUSTERS
  There are  13 clusters, with trajectories as follows:
   16   15   15   15   15   15   15   15   15   15   15   15   15
  clusterdelta =  0.800E-03
  clustereps =  0.183E-07
 OUTPUT
   data files 'sol.txt' and 'loc.txt' have been written.
 RESULT
   large small eps delta
   3   10 .800E-03 .183E-07
```

If plotting is enabled, a Python script is executed after the computations have finished to plot the solution in phase space and time as shown in Fig. 13.
`bif.f90` supports calculations over ranges of parameter values. For this one has to prescribe the left and right endpoints of the interval as well as the number of grid points. For example, changing b from 0.017 to 0.02 yields the transition from a 3^{10}-type to a 4^{19}-type MMO. The corresponding output of `bif.f90` is:

```
# ./bif b=0.017,0.020,10
# BIF -- $Revision: 1.16 $
#   par(2)
 0.017000000    3   10 .800E-03 .183E-07
 0.017333333    2    7 .110E-02 .291E-12
 0.017666667    0    0 .100E-03 .709E-04
```

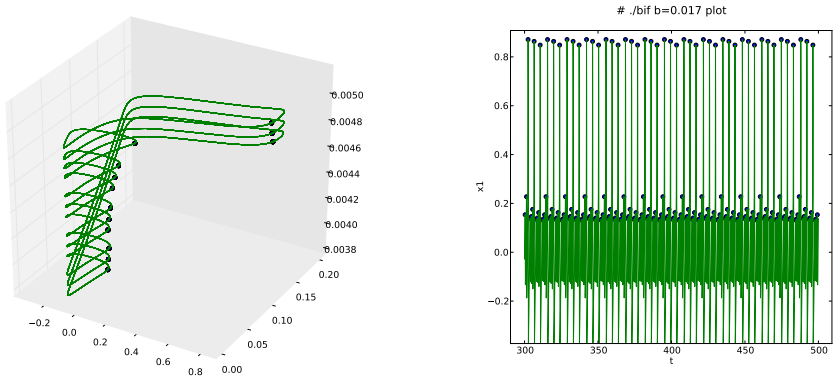

Fig. 13 These graphics are generated from the data in the files `sol.txt` and `loc.txt` when using the command line `./bif b=0.017 plot`

```
 0.018000000    0    0 .102E-03 .000E+00
 0.018333333    1    4 .352E-02 .249E-11
 0.018666667    0    0 .121E-03 .371E-10
 0.019000000    0    0 .108E-03 .417E-04
 0.019333333    3   13 .403E-03 .576E-05
 0.019666667    2    9 .774E-03 .267E-11
 0.020000000    4   19 .339E-03 .304E-09
```

If the user provides ranges for more than one parameter, `bif.f90` will automatically loop over all possible combinations. For example, to change b and K simultaneously, one can use `bif.f90` as follows:

```
# ./bif b=0.017,0.020,3 K=0.3,2,3
# BIF -- $Revision: 1.16 $
#   par(2)     par(3)
 0.017000000  0.300000000    3   10 .800E-03 .183E-07
 0.017000000  1.150000000    2    5 .132E-02 .353E-08
 0.017000000  2.000000000    0    0 .104E-03 .483E-05
 0.018500000  0.300000000    1    4 .299E-02 .159E-11
 0.018500000  1.150000000    1    3 .417E-03 .249E-05
 0.018500000  2.000000000    0    0 .101E-03 .277E-07
 0.020000000  0.300000000    4   19 .339E-03 .304E-09
 0.020000000  1.150000000    0    0 .101E-03 .000E+00
 0.020000000  2.000000000    0    0 .117E-03 .137E-06
```

Reports of the Institutes 2010

01-10. Kristian Debrabant, Anne Kværnø, *B-series analysis of iterated Taylor methods*

02-10. Jan Prüss, Mathias Wilke, *On conserved Penrose-Fife type models*

03-10. Bodo Dittmar, *Maxima for the expectation of the lifetime of a Brownian motion in the ball*

04-10. M. Köhne, J. Prüss, M. Wilke, *Qualitative behaviour of solutions for the two-phase Navier-stokes equations with surface tension*

05-10. R. Weiner, G. Kulikov, H. Podhaisky, *Variable-stepsize doubly quasi-consistent parallel explicit peer methods with global error control*

06-10. T. El-Azab, R. Weiner, *Exponential peer methods with variable step sizes*

07-10. St. Beck, R. Weiner, H. Podhaisky, B. A. Schmitt, *Implicit peer methods for large stiff ODE systems*

08-10. Ch. Tammer, C. Zălinescu, *Minimal-Point Theorems in Product Spaces and Applications*

09-10. A. Khan, Ch. Tammer, *Regularization of Quasi Variational Inequalities*

Reports are available via WWW: http://www2.mathematik.uni-halle.de/institut/reports/